Kinetic Monte Carlo simulation of faceted islands in heteroepitaxy using multi-state lattice model

Chi-Hang Lam

Department of Applied Physics, Hong Kong Polytechnic University, Hung Hom, Hong Kong, China

(Dated: September 9, 2009)

A solid-on-solid model is generalized to study the formation of Ge pyramid islands bounded by (105) facets on Si(100) substrates in two dimensions. Each atomic column is not only characterized by the local surface height but also by two deformation state variables dictating the local surface tilt and vertical extension. These deformations phenomenologically model surface reconstructions in (105) facets and enable the formation of islands which better resemble faceted pyramids. We demonstrate the model by application to a kinetic limited growth regime. We observe significantly reduced growth rates after faceting and a continuous nucleation of new islands until overcrowding occurs.

I. INTRODUCTION

Strain induced self-assembly of three dimensional (3D) islands in heteroepitaxy have been attracting much research interest because of the rich physics involved and their potential applications as quantum dots in optoelectronic devices [1, 2, 3]. A widely studied system is Ge deposited on Si(100) substrates with a 4% lattice misfit. Relatively flat islands in the form of stepped mounds with unfaceted sidewalls called pre-pyramids start to emerge at 3 monolayers (MLs) of Ge coverage [4, 5]. Further deposition leads to pyramids or rectangular-based huts bounded by (105) facet planes. Deposition temperatures lower than $500°C$ generally favors rectangular huts [6, 7] while higher temperature often leads to pyramids [8]. After still further deposition or annealing, pyramids can grow into dome islands bounded mainly by steeper (113) facets [9, 10].

(105) facets on pyramids and huts have been found to be extraordinarily stable and atomically flat from first principle calculations [11, 12, 13, 14]. At low temperature, surface steps on (105) facets are rarely observed [7]. They are however present at higher temperature and the bunching of them are observed to be important to the morphological evolution [15]. The structures, energies and dynamics of these steps have been studied using first-principles calculations [16]. Also, the edge energies of a (105) faceted ridge have been estimated using molecular dynamics simulations based on empirical potentials [17].

Large scale simulations of the formation of 3D islands is possible using kinetic Monte Carlo (KMC) methods based on lattice models [18, 19, 20, 21, 22, 23, 24, 25, 26, 27]. The simulations are computationally very intensive due to the long-range nature of elastic interactions. Elastic forces can be accounted for accurately and efficiently using advanced algorithms so that simulations in 2D [21, 22] and 3D [23, 24, 25, 26] with respectively large and moderate system sizes are possible. Using more approximate forms of the elastic interactions, larger systems in 3D can also be studied [20, 27].

KMC studies on strained layers are generally based on square or cubic lattices for simplicity. Strain induced islands or pits are readily generated but their sidewalls are almost vertical [18, 24, 26] or at an of inclination of about 45 degrees [19, 21, 23, 27] depending on the details of the bond energies or additional constraints used. These inclinations are much steeper than 11° and 26° for the (105) and (113) facets respectively. The realistic facets however are of rather low-symmetry and in general are not favored energetically in lattice models. The discrepancy results in strain distributions considerably different from the realistic ones and may probably lead to qualitatively different growth modes in certain situations. Furthermore, the surface energy of the island sidewalls from existing KMC models are not independently adjustable and there is no simple approach to incorporate for example the extraordinary stability of certain facets. In addition, with only one favored sidewall slope in a given model, only one type of island can be simulated so that studying the pyramid to dome transition for instance is impossible.

In this work, we extend the convectional ball and spring lattice model for KMC simulation of heteroepitaxial solids in 2D by allowing specific geometrical deformation states of the surface atoms. These deformations phenomenologically represent surface reconstructions on (105) facets. We show computationally that this new multi-state model leads to the formation of faceted islands. Examples of qualitative differences in the growth dynamics between faceted and unfaceted islands are explained.

II. BALL AND SPRING LATTICE MODEL

We first explain the conventional square lattice model of elastic solids in 2D while further extensions will be introduced in the next section. Every atom is associated with a lattice sites and are connected to nearest and next nearest neighbors by elastic springs. Solid-on-solid conditions are assumed. We follow the model parameters

used in Ref. [21] unless otherwise stated to approximate the widely studied Ge/Si(001) system. We assume a substrate lattice constant $a_s = 2.715$Å so that a_s^3 gives the correct atomic volume in crystalline silicon. The lattice misfit $\epsilon = (a_f - a_s)/a_f$ equals 4% where a_f is the lattice constant of the film. Nearest and next nearest neighboring atoms are directly connected by elastic springs with force constants $k_N = 13.85eV/a_s^2$ and $k_{NN} = k_N/2$ respectively. The elastic couplings of adatoms with the rest of the system are weak and are completely neglected for better computational efficiency. In this model, surface steps have a particularly high tendency to bunch together under strain presumably due to the much weaker entropic surface step repulsion in 2D. We hence forbid double surface steps as well as adjacent single surface steps of the same direction so that the steepest surface slope allowed is 1/2.

The KMC approach simulates the morphological evolution by explicitly considering the diffusion of surface atoms. Every topmost atom m on the film can hop to a nearby site with a hopping rate $\Gamma(m)$ following an Arrhenius form:

$$\Gamma(m) = R_0 \exp\left[-\frac{n_m\gamma - \Delta E_s(m) - E_0}{k_B T}\right] \quad (1)$$

where n_m is the number of nearest and next nearest neighbors of atom m. We have assumed an identical nearest and next nearest neighbor bond strength γ. We put $\gamma = 0.5eV$, slightly larger than the value in Ref. [21] so that the energy costs of stepped mounds become slightly higher. The energy $\Delta E_s(m)$ is the difference in the strain energy E_s of the whole lattice at mechanical equilibrium with or without the atom m. Due to the long-range nature of elastic interactions, its efficient calculation is highly nontrivial and we handle it using a Green's function method together with a super-particle approach explained in Refs. [21, 25, 28]. In addition, $E_0 = 3\gamma - 0.67eV$, where 0.67eV is the adatom diffusion barrier on the (100) plane. To speed up the simulations, long jumps are allowed so that a hopping atom will jump directly to another random topmost site at most $s_{max} = 8$ columns away with equal probability. Then, $R_0 = 2D_0/(\sigma_s a_s)^2$ with $D_0 = 3.83 \times 10^{13}$Å$^2 s^{-1}$ and $\sigma_s^2 = \frac{1}{6}(s_{max} + 1)(2s_{max} + 1)$. This gives the appropriate adatom diffusion coefficient for silicon (100).

III. MULTI-STATE LATTICE MODEL WITH SURFACE DEFORMATION

To effectively model (105) facets, which are more precisely (15) surfaces in 2D, we introduce additional degrees of freedom representing local deformations to all topmost atoms. They phenomenologically accounts for the surface rebonding or reconstruction states on a (105) faceted region [11]. For efficient computation, these deformations localized to individual surface atoms are assumed to be completely independent of the lattice misfit,

although correlations between misfit strain and surface reconstruction are known to exist, [12, 13, 14]. In the following calculation of the local deformation energies, we hence neglect lattice misfit and express all lengths in unit of lattice constant. The subsequent calculation of the misfit strain energy term is identical to that outlined in Sec. II.
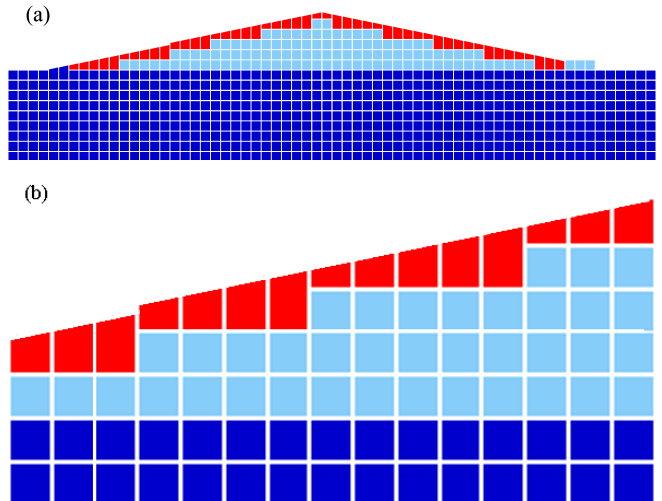

FIG. 1: A faceted island from a small scale simulation using the multi-state model (a) and a magnification of part of the surface containing a (105) surface step between the third and the fourth columns (b). Deformed film atoms, undeformed film atoms and all substrate atoms are shaded in red, light blue and dark blue respectively. In (b), the tilt variable σ_i is $\frac{1}{5}$ for all columns, while the extension variable κ_i from left to right equals $0, \frac{1}{5}, \frac{2}{5}, -\frac{1}{5}, 0, \frac{1}{5}, \frac{2}{5}, -\frac{2}{5}, -\frac{1}{5}, 0, \frac{1}{5}, \frac{2}{5}, -\frac{2}{5}, -\frac{1}{5}$ and 0.

We first show an example of a faceted island from a small scale simulation in Fig. 1(a). Figure 1(b) magnifies part of the surface. It shows how the surface deformation smooths out the (100) steps of the original stepped mound and turn the sidewalls into atomically flat effective (105) facets with slopes $\pm 1/5$. An example of a surface step on the (105) surface is also shown and will be explained later. In the absence of deformation, an atom is represented by a unit square. An integer h_i denotes the surface height at column i. We assume that a topmost atom in the film surface or in an exposed region of the substrate can be deformed into a trapezoid characterized by two new deformation state variables, namely a tilt variable σ_i and an extension variable κ_i. We put

$$\sigma_i = 0, \ \frac{1}{5}, \ \text{or} \ -\frac{1}{5} \quad (2)$$

which gives the slope of the upper surface of the deformed atom. The values $\sigma_i = \pm 1/5$ enable the formation of the (105) facets in both directions. As shown in Fig. 1(b), attaining a flat (105) faceted region further requires properly coordinated vertical stretching or compression

of the topmost atom by κ_i which is given by

$$\kappa_i = \begin{cases} 0 & \text{for } \sigma_i = 0 \\ -\frac{2}{5}, -\frac{1}{5}, 0, \frac{1}{5}, \text{ or } \frac{2}{5} & \text{for } \sigma_i = \pm\frac{1}{5} \end{cases} \quad (3)$$

The ith atomic column hence can be rectangular or trapezoidal with the left and right edges of heights h_i^a and h_i^b given by

$$h_i^a = h_i + \kappa_i - \frac{\sigma_i}{2} \quad (4)$$

$$h_i^b = h_i + \kappa_i + \frac{\sigma_i}{2} \quad (5)$$

A surface step in between the ith and the $(i+1)$th column has a step height δ_i defined as

$$\delta_i = | h_{i+1}^a - h_i^b | \quad (6)$$

For simplicity, we have measured step heights as projected along the lattice axis rather than the surface normals. Note that single steps on (100) and (105) surfaces have very different heights of 1 and 1/5 respectively in our model.

We will next explain the energy cost of the local deformation of the surface atoms. Values of the energy parameters to be introduced are chosen phenomenologically to provide morphologies best compared with observations. Similar to the original lattice model [21], although we believe that our parameters are within physically acceptable ranges, this model being in 2D is not realistic enough to apply directly parameters from first principle studies [12, 13, 14] in general. Furthermore, we have found from numerous exploratory simulations that only a rather limited and specific range of parameters provides reasonable morphologies under a wide range of relevant growth conditions. The constraints on our parameters hence may also shed light on how the morphologies reveals certain features on the microscopic details of the surface and this will be discussed further.

The hopping rate of a topmost atom m in Eq. (1) is generalized to

$$\Gamma(m) = R_0 \exp\left[\frac{\Delta E_b(m) + \Delta E_s(m) + E_0'}{k_B T}\right] \quad (7)$$

where $E_0' = -\gamma - 0.67$ eV. The misfit strain energy term $\Delta E_s(m)$ is defined similarly as before and its calculation is assumed to be completely independent of the local surface deformation. The surface energy term $\Delta E_b(m)$ denotes the change in the bond energy E_b of the whole surface when the site is occupied versus unoccupied. More precisely, surface energy is defined relative to that of a flat (100) surface as

$$E_b = \sum_i [\eta(\sigma_i) + \nu(\sigma_i, \sigma_{i+1}) + \omega(\delta_i, \sigma_i, \sigma_{i+1})] \quad (8)$$

Here, $\eta(\pm 1/5) = 5$ meV is the formation energy per site of the (105) facet and $\eta(0) = 0$ for the (100) region. Also,

$\nu(\sigma_i, \sigma_{i+1}) = 0.35$ eV denotes the interface energy at the boundary of a facet where $\sigma_i \neq \sigma_{i+1}$ and it is zero otherwise. It dictates the energy barrier of facet nucleation. If we choose a larger value of $\eta(\pm 1/5)$, the (105) facet can become unstable. A negative value of $\eta(\pm 1/5)$ has been suggested [14] corresponding to extremely stable (105) facets. However, this is not acceptable as island sizes from such simulations are then dominated by ν closely related to the edge energy in Ref. [14] but is practically independent of the lattice misfit.

The last term in Eq. (8) represents the energy of a surface step. On a (100) region with $\sigma_i = \sigma_{i+1} = 0$, it is defined as

$$\omega(\delta_i, \sigma_i, \sigma_{i+1}) = \frac{\gamma}{2}\delta_i \quad (9)$$

where the step height δ_i defined in Eq. (6) is a integer. This results from simple bond counting noting that two single steps are created by breaking one nearest neighboring bond of strength γ. Noting also that a bulk atom has a bond energy of -4γ, Eq. (7-9) reduces exactly to Eq. (1) so that the (100) regions in the multi-state model behaves identically to the basic model in Sec. II. Outside of a (100) region (i.e. σ_i or $\sigma_{i+1} \neq 0$) we put

$$\omega(\delta_i, \sigma_i, \sigma_{i+1}) = \beta_{105}\left(1 + \chi - \chi e^{1-5\delta_i}\right) + \frac{\gamma}{2}\left(\delta_i - \frac{1}{5}\right) \quad (10)$$

for $\delta_i \geq 1/5$ and it is zero otherwise. This expression gives an energy β_{105} for a single step with height $\delta_i = 1/5$ on a (105) region. It is known that incomplete (105) facets can be practically absent at low temperature around $450°C$ [7] but are observable at $550°C$ [15]. We reproduce this feature in our model by taking a relatively large value of $\beta_{105} = 0.3$ eV. From Eq. (10), the step energy per unit height of a multiple step approaches $\gamma_n/2$ identical to that for a step on a (100) facet. This also reduces the energy of an adatom on a (105) surface which is bounded by two unit steps to a more acceptable but still very large value of 1.3 eV. The parameter χ determines the energy of multiple steps of intermediate heights. We put $\chi = 0.5$ allowing a slight tendency of step bunching [15].

In KMC simulation using this multi-state model, the atomic hopping events are randomly sampled and simulated according to the rates $\Gamma(m)$ in Eq. (7). We assume that the deformation state variables σ_i and κ_i at every column are unchanged after an atomic hop, i.e. the deformation state is attached to the column rather than to the hopping atom. Deposition of an atom also increases the column height by unity without altering the deformation state. After every period τ, the deformation state for a set of columns will be updated. Specifically, to facilitate program parallelization, we adopt a sublattice updating scheme in which the deformation states at all odd (even) lattice sites will be updated at every odd (even) updating event. When column i is to be updated, the variables σ_i and κ_i are re-sampled from the allowed set of 11 possible combinations using a heat bath algorithm based on the

relative probability $exp(-E_b/kT)$. We take $\tau = 2/\Gamma_{ad}$ where Γ_{ad} is the adatom hopping rate on a (100) surface easily calculable from Eq. (1). This is the highest possible rate without increasing significantly the overall execution time of our program. Local changes in the surface reconstruction states are most likely a fast process compared with atomic hopping. We have checked that our deformation state updating rate is indeed sufficiently fast so that decreasing τ gives no observable difference to our results. Our model follows detailed balance which allows us to confirm the reliability of our software implementation using a Boltzmann's distribution test [25].

IV. RESULTS

Using both the conventional ball and spring lattice model and the multi-state lattice model with surface deformation explained in Secs. II and III, we have simulated the self-assembly of strained islands in 2D. A substrate of size 1024×1024 (width $\times$ depth) is used. We take a temperature $450°$ and a deposition rate 0.1 ML/s. The conventional and the multi-state models lead to islands with unfaceted and faceted sidewalls respectively. For convenience, we refer to them as unfaceted and faceted islands.

Figure 2(a) shows the evolution of unfaceted islands from a typical run using the conventional model during deposition of up to 6 MLs of film material on to an initially flat substrate. Unstable shallow stepped mounds develop at very early stage. After depositing about 2 MLs, some stepped mounds have attained steeper sidewalls and become more stable. At about 4 MLs, they have generally attained the steepest possible slope of $1/2$ allowed in our model. As observed in this and other similar runs, there is a rather well defined island nucleation period and no new island emerges after some larger islands are established. We also observe that some relatively mature islands eventually decay and vanish, indicating a ripening process. The existence of a finite nucleation period followed by ripening is consistent with previous KMC simulations [27] as well as continuum simulations [29, 30]. It may also have some experimental relevance at higher temperature although the pyramid to dome transition and alloying between the film and substrate atoms [10] add further complications.

Analogous evolution of faceted islands simulated using the multi-state model with surface deformation is shown in Fig. 2(b). Small highly unstable (105) faceted regions with deformed surface atoms begin to appear at a coverage of about 0.5 MLs. Relatively stable (105) faceted islands emerges at about 1 ML. These islands develops from the larger ones of the stepped mounds. Faceted regions nucleate on either side of the mounds independently so that half faceted asymmetric islands exist during the course of development. Islands also often go through an truncated pyramid stage [5] with unfaceted tops before finally becoming fully developed pyramids.
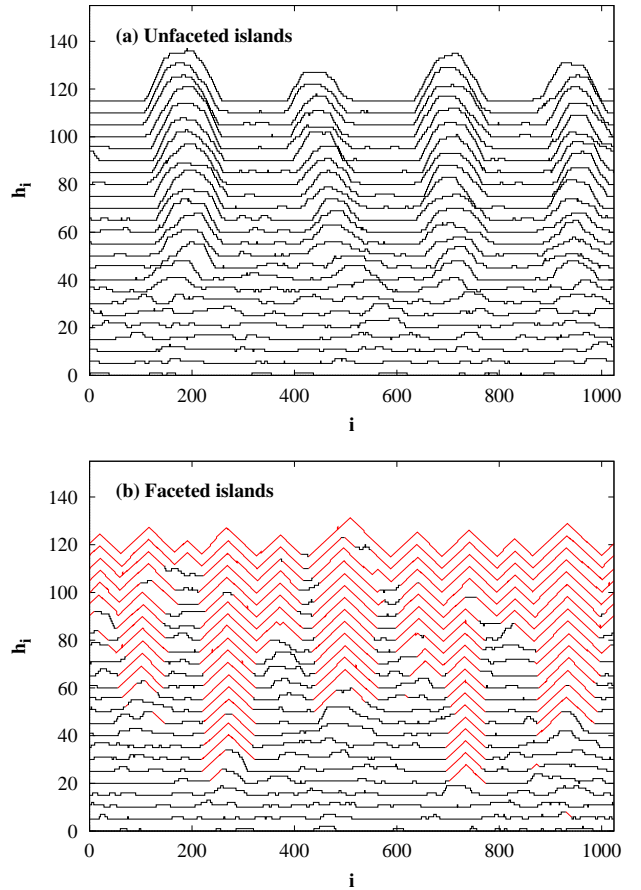

FIG. 2: Snapshots of surfaces showing the development of (a) unfaceted and (b) faceted islands simulated respectively using the conventional model and the multi-state model. (105) faceted regions are shaded in red. Each successive profile is displaced by +5 vertically for clarity and corresponds to the deposition of a further 1/4 MLs up to a total of 6 MLs.

Some faceted islands may occasionally decay partially or even completely back to unfaceted stepped mounds, but the larger ones are much more stable. On the other hand, some stepped mounds may happen to get faceted at rather small sizes while slightly larger ones can remain unfaceted for long periods. Therefore, the faceting process in our current model is strongly affected by both the energetics and the kinetics.

At this low growth temperature of $450°$, surface steps on a (105) facet is rare as explained in Sec. III. Further growth of faceted islands by step flow is hence kinetic limited [6, 7]. It can be observed from Fig. 2(b) that island growth rates drop dramatically once becoming faceted. Their sizes occasionally jump up rapidly only when parts of the sidewalls become temporarily unfaceted due to thermal excitation. Since developed islands are poor absorber of newly deposited atoms, new islands continue to nucleate until the substrate is crowded with islands. Kinetic limited growth and continuous island nucleation have not been reported previously in KMC or continuum

simulations in our knowledge. More importantly, deposition experiments at 550°C do indicate slower growth of matured islands and a continuous island nucleation growth mode [8]. Deposition at lower temperature however leads to huts [6, 7] which may share some related characteristics but are more complicated.
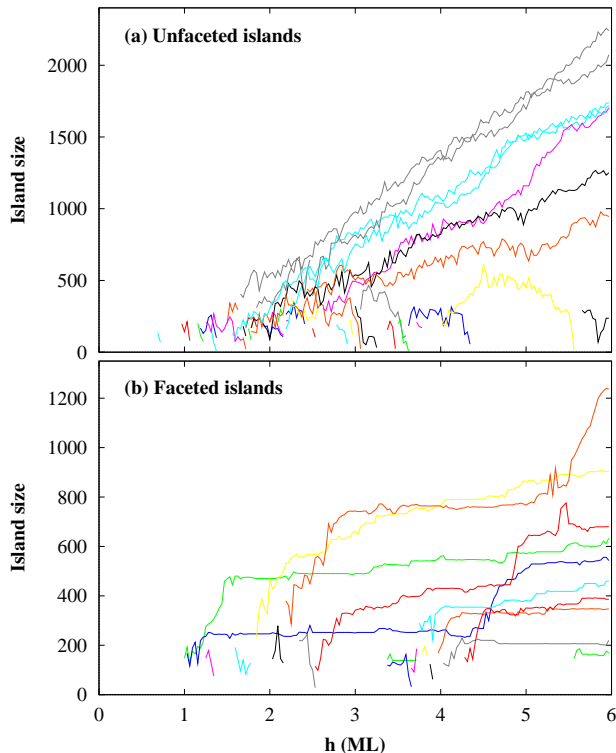

FIG. 3: Plot of island size against nominal film thickness h for unfaceted (a) and faceted (b) islands

For more quantitative analysis, we define an island as one in which each of the constituent columns must be at least 4 atoms tall. All islands can then be automatically identified. Figure 3 traces the size evolution against the nominal film thickness h of every island in Fig. 2 once they have attained a size of at least 150 atoms. Islands from another similar run are also included in Fig. 3(b) to provide additional examples. From Fig. 3(a), unfaceted islands beyond a certain size in general grow steadily with its own characteristic rates which are expected to depend mainly on the sizes of their adatom capture zones. Small islands decay and vanish. In contrast, from Fig. 3(b), there is in general an initial period of rapid island growth followed by much slower growth after faceting. Once faceted, their sizes remain nearly constant except at occasional jumps associated with temporary partial decay of the facets as described above.

To obtain more statistics, we have repeated each simulation 200 times. Figure 4 plots the average number of islands of size 150 or larger on the 1024 atoms wide sub-
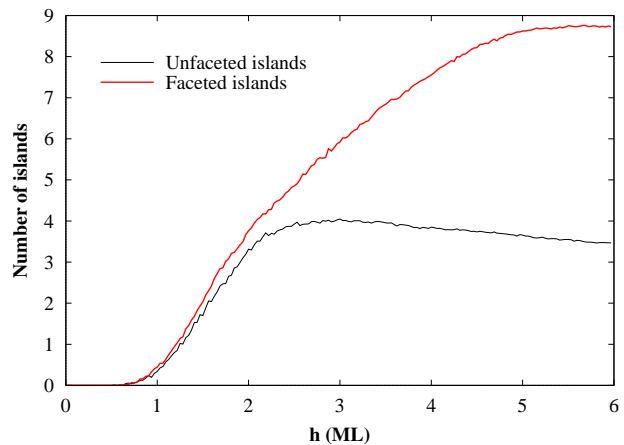

FIG. 4: Plot of the average number of islands on a substrate of 1024 atoms wide against nominal film thickness h

strate used. Smaller islands are excluded because they are highly unstable. For unfaceted islands, their number first increases indicating a period of active nucleation at coverage from about 1 to 2.5 MLs. It then declines but at a very slowly rate indicating rather inefficient coarsening during growth. In contrast, faceted islands steadily increase in number for coverage up to about 5 MLs due to continuous nucleation. Beyond 5 MLs, the substrate is crowded with islands and the number of islands saturates.

Finally, we histogram the island sizes from all the independent runs. Fig. 5 plots the average number of islands on the substrate against island size. For both models, a peak island size emerges for $h \gtrsim 2.5$ MLs. For unfaceted islands, the histogram broadens significantly upon growth due to a wide distribution of growth rates. In contrast for faceted islands, it broadens much more slowly due to the highly kinetic limited growth mode. Nevertheless, the faceted islands do not possess narrower size distribution relative to the average size. This is because a significant size distribution already exists when the islands become faceted as can be observed in Fig. 2(b). The continuous nucleation of new islands also broadens the distribution as the older islands are larger on average. Another difference between the models is that the peak of the histogram decays monotonically upon deposition for unfaceted islands while it increases for $2.5 \leq h \leq 4.5$ due to the continuous nucleation of islands.

V. DISCUSSIONS

We have generalized a lattice model for strained films to allow for a range of local deformation states of surface atoms representing effective surface reconstructions. This deformations are assumed to be independent of the misfit induced strains for simplicity. Using this multi-
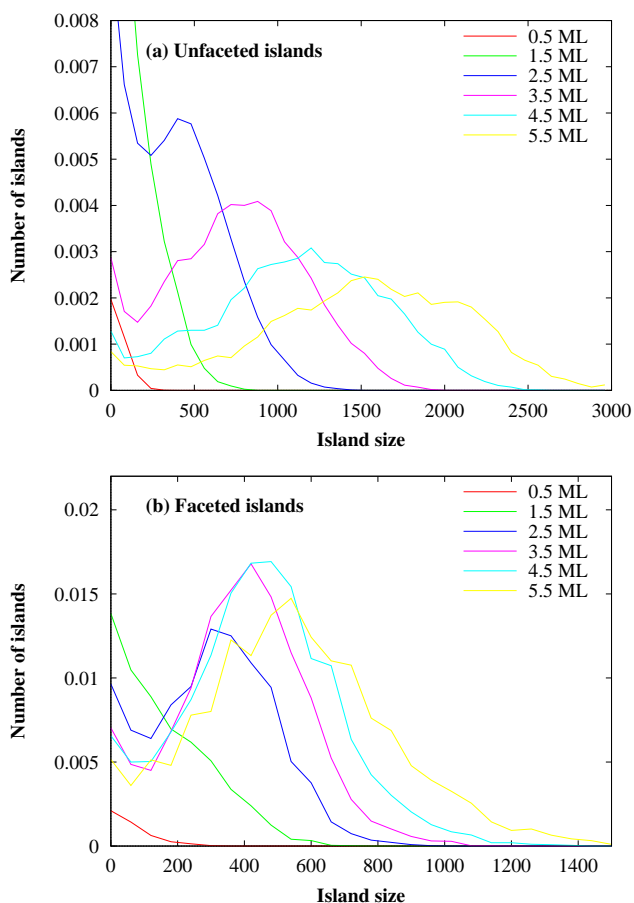
state lattice model, we have performed kinetic Monte Carlo simulations in 2D and observed the formation of (105) faceted pyramid islands. The model enables us to simulate faceted island formation in the kinetic limited regime. In this regime, island growth slows down dramatically and becomes intermittent after faceting. The slower growth of the more established islands also leads to a continuous nucleation of islands until the substrate is fully occupied. The width of the island distribution is dominated both by fluctuations in the initial size at the start of faceting as well as the diversity in their ages. Stepped mounds from the conventional model exhibit a simple nucleation period followed by slow ripening.

Additional studies on the growth and annealing of faceted islands under other growth conditions will be report elsewhere. It is also interesting to further generalize the model to consider two facet types so as to study the pyramid to dome transition. Generalization to 3D is conceptually straightforward but is challenging in practice because of the heavy computational load expected.

FIG. 5: Size histograms for unfaceted (a) and faceted (b) islands

[1] P. Politi, G. Grenet, A. Marty, A. Ponchet, and J. Villain, Phys. Rep. **324**, 271 (2000).
[2] V. A. Shchukin, N. N. Ledentsov, and D. Bimberg, *Epitaxy of nanostructures* (Springer, 2003).
[3] I. Berbezier and A. Ronda, Surf. Sci. Rep. **64**, 47 (2009).
[4] Y.-W. Mo, D. E. Savage, B. S. Swartzentruber, and M. G. Lagally, Phys. Rev. Lett. **65**, 1020 (1990).
[5] A. Vailionis, B. Cho, G. Glass, P. Desjardins, D. G. Cahill, and J. E. Greene, Phys. Rev. Lett. **85**, 3672 (2000).
[6] M. Kästner and B. Voigtländer, Phys. Rev. Lett. **82**, 2745 (1999).
[7] M. R. Mckay, J. A. Venables, and J. Drucker, Phys. Rev. Lett. **101** (2008).
[8] A. Rastelli and H. von Kanel, Surf. Sci. **532**, 769 (2003).
[9] G. Medeiros-Ribeiro, A. Bratkovski, T. Kamins, D. Ohlberg, and R. Williams, Science **279**, 353 (1998).
[10] A. Rastelli, M. Stoffel, J. Tersoff, G. S. Kar, and O. G. Schmidt, Phys. Rev. Lett. **95**, 026103 (2005).
[11] Y. Fujikawa, K. Akiyama, T. Nagao, T. Sakurai, M. G. Lagally, T. Hashimoto, Y. Morikawa, and K. Terakura, Phys. Rev. Lett. **88**, 176101 (2002).
[12] S. Cereda, F. Montalenti, and L. Miglio, Surf. Sci. **591**, 23 (2005).
[13] G.-H. Lu, M. Cuma, and F. Liu, Phys. Rev. B **72**, 125415 (2005).
[14] O. Shklyaev, M. Beck, M. Asta, M. Miksis, and P. Voorhees, Phys. Rev. Lett. **94** (2005).
[15] F. Montalenti, P. Raiteri, D. Migas, H. von Kanel, A. Rastelli, C. Manzano, G. Costantini, U. Denker, O. Schmidt, K. Kern, et al., Phys. Rev. Lett. **93** (2004).
[16] S. Cereda and F. Montalenti, Phys. Rev. B **75**, 195321 (2007).
[17] C. M. Retford, M. Asta, M. J. Miksis, P. W. Voorhees, and E. B. Webb III, Phys. Rev. B **75**, 075311 (2007).
[18] B. G. Orr, D. Kessler, C. W. Snyder, and L. Sander, Europhys. Lett. **19**, 33 (1992).
[19] K. E. Khor and S. Das Sarma, Phys. Rev. B **62**, 16657 (2000).
[20] M. Meixner, E. Scholl, V. Shchukin, and D. Bimberg, Phys. Rev. Lett. **88** (2002).
[21] C.-H. Lam, C.-K. Lee, and L. M. Sander, Phys. Rev. Lett. **89**, 216102 (2002).
[22] J. L. Gray, R. Hull, C.-H. Lam, P. Sutter, J. Means, and J. A. Floro, Phys. Rev. B **72**, 155323 (2005).
[23] M. T. Lung, C.-H. Lam, and L. M. Sander, Phys. Rev.

Lett. **95**, 086102 (2005).

[24] G. Russo and P. Smereka, J. Comput. Phys. **214**, 809 (2006).

[25] C.-H. Lam, M. T. Lung, and L. M. Sander, J. Sci. Comput. **37**, 73 (2008).

[26] J. Y. Lee, M. J. Noordhoek, P. Smereka, H. McKay, and J. M. Millunchick, Nanotechnology **20** (2009).

[27] R. Zhu, E. Pan, and P. W. Chung, Phys. Rev. B **75**

[28] C.-H. Lam and M. T. Lung, Int. J. Mod. Phys. B **21**, 4219 (2007).

[29] P. Liu, Y. Zhang, and C. Lu, Phys. Rev. B **68** (2003), ISSN 1098-0121.

[30] J.-N. Aqua, T. Frisch, and A. Verga, Phys. Rev. B **76** (2007).

(2007).